Research Article

Cancer Immunology Research

Combination of CD40 Agonism and CSF-1R Blockade Reconditions Tumor-Associated Macrophages and Drives Potent Antitumor Immunity

Karla R. Wiehagen[1], Natasha M. Girgis[1,2], Douglas H. Yamada[1], Andressa A. Smith[1], Szeman Ruby Chan[1], Iqbal S. Grewal[1], Michael Quigley[1,3], and Raluca I. Verona[1]

Abstract

Efficacious antitumor immune responses must overcome multiple suppressive mechanisms in the tumor microenvironment to control cancer progression. In this study, we demonstrate that dual targeting of suppressive myeloid populations by inhibiting CSF-1/CSF-1R signaling and activation of antigen-presenting cells with agonist anti-CD40 treatment confers superior antitumor efficacy and increased survival compared with monotherapy treatment in preclinical tumor models. Concurrent CSF-1R blockade and CD40 agonism lead to profound changes in the composition of immune infiltrates, causing an overall decrease in immunosuppressive cells and a shift toward a more inflammatory milieu. Anti-CD40/anti–CSF-1R–treated tumors contain decreased tumor-associated macrophages and Foxp3$^+$ regulatory T cells. This combination approach increases maturation and differentiation of proinflammatory macrophages and dendritic cells and also drives potent priming of effector T cells in draining lymph nodes. As a result, tumor-infiltrating effector T cells exhibit improved responses to tumor antigen rechallenge. These studies show that combining therapeutic approaches may simultaneously remove inhibitory immune populations and sustain endogenous antitumor immune responses to successfully impair cancer progression. *Cancer Immunol Res; 5(12); 1109–21. ©2017 AACR.*

Introduction

To escape detection by the immune system, tumors foster an immunosuppressive environment and produce signals that subdue antitumor immune responses (1). Tumor-associated macrophages (TAMs) are a heterogeneous population of myeloid cells that differentiate in the tumor microenvironment and become sensitized to tumor-derived suppressive signals (2). TAMs, in turn, act to prevent local immune responses by inefficiently presenting antigen and generating suppressive signals such as IL10, indoleamine-pyrrole 2,3-dioxygenase (IDO), and TGFβ that inhibit lymphocyte function and metabolism (3). Therefore, for adaptive immune responses to persist, tumor-infiltrating lymphocytes (TILs) must overcome a suppressive cytokine milieu and mechanisms of tolerance propagated by TAMs to successfully attack cancerous cells.

CSF-1 (M-CSF) is a cytokine that supports differentiation, proliferation, and function of monocyte and macrophage populations (4). In tumors, CSF-1 promotes immune suppression by expanding and promoting differentiation of myeloid-derived suppressor cells (MDSC) and alternatively activated MHC II^{lo} TAMs that express its cognate receptor, CSF-1R (5, 6). High CSF-1R expression on infiltrating immune cells in the TME correlates with immune dysfunction and increased immunosuppression (7, 8), as well as poor prognosis in breast, ovarian, pancreatic cancers, and lymphoma (9–11). Although inhibiting the CSF-1/CSF-1R axis alone constrains tumor growth in preclinical models by partially decreasing TAMs and encouraging T-cell infiltration (12–16), it has often proven insufficient to clear tumors. Pairing CSF-1R blockade with chemotherapeutic agents or checkpoint inhibitors has enhanced efficacy of the monotherapy activity of CSF-1R (17).

CD40 is a highly conserved costimulatory receptor expressed on antigen-presenting cells (APCs) including dendritic cells (DC), macrophages, monocytes, B cells, as well as a number of non-hematopoietic cell types and some tumor cells (18, 19). The ligand for CD40 (CD40L) is expressed on activated T cells and B cells and, under inflammatory conditions, is upregulated on innate immune cells as well as endothelial and epithelial cells (20–24). CD40 ligation drives "licensing" (maturation and activation) of APCs, enabling effective antigen presentation and stimulation of CD4$^+$ Th1 and CD8$^+$ T cells. This is a key step in mounting antitumor responses, as supported by emerging preclinical and clinical data with agonist anti-CD40 in multiple tumor types (18, 20, 25). However, a number of studies have shown that potency of CD40 agonists can be enhanced by combinations with other immune modulatory therapies such as TLR agonists, cytokines including type I interferons and IL2, adoptive cell transfer, and chemotherapy (18, 26–30). A study

[1]Janssen Research and Development, Spring House, Pennsylvania. [2]Constellation Pharmaceuticals, Cambridge, Massachusetts. [3]Bristol-Myers Squibb, Princeton, New Jersey.

Note: Supplementary data for this article are available at Cancer Immunology Research Online (http://cancerimmunolres.aacrjournals.org/).

Corresponding Author: Raluca I. Verona, Janssen R&D, 1400 McKean Road, Spring House, PA 19477. Phone: 215 628-5211; E-mail: rverona@its.jnj.com

doi: 10.1158/2326-6066.CIR-17-0258

also demonstrated that CD40 agonism following CSF-1R blockade leads to enhanced antitumor efficacy, suggesting these two therapies may cooperate when coadministered (30).

In this study, we sought to investigate whether dual targeting of suppressive myeloid populations via CSF-1/CSF-1R inhibition and APC activation with agonist anti-CD40 treatment confers enhanced antitumor efficacy compared with monotherapy treatments. Tumor profiling after anti-CD40/anti–CSF-1R treatment revealed significant changes in the composition of $CD11b^+$ myeloid populations, decreased frequencies of regulatory $Foxp3^+$ T cells (Treg), and increased infiltration of effector TILs. Analysis of the cytokine milieu in combination-treated tumors demonstrated an inflammatory TME, which corresponded with improved control of tumor burden. The combination of starving TAMs while activating APCs resulted in a cascade of proinflammatory responses and significant gains in effector T-cell responses and tumor clearance. Thus, the combination of anti-CD40 and anti–CSF-1R simultaneously removes inhibitory immune populations and drives endogenous antitumor immune responses to improve tumor clearance and significantly lengthen overall survival.

Materials and Methods

Tumor cell lines

CT26 and MC-38 cell lines were obtained from ATCC. Cell lines were authenticated and certified by ATCC (February 2015) and regularly tested by Analytical Biological Services, Inc. MAP/RAP PCR results (February 2016) were negative, and <1 EU/mL by limulus amebocyte lysate (LAL; ATCC, ABS). CT26 and MC-38 cell lines were cultured *in vitro* under conditions specified by the ATCC and passaged up to 3 times before implant.

Syngeneic tumor studies

In all *in vivo* studies, age-matched female mice from Charles River Laboratories were implanted subcutaneously with 5×10^5 cultured cells of the indicated tumor line suspended in PBS. Animal welfare (grooming, activity) was monitored daily, and animal weights and caliper measurements to calculate tumor volume ($L \times L \times W/2$) were collected at least twice per week until end of the study or until tumor burden limit approached 2,000 mm^3. All studies were conducted in accordance with internal Institutional Animal Care and Use Committees of Janssen R&D and in compliance with federal guidelines.

Female Balb/c mice, 6 to 9 weeks old, bearing subcutaneous CT26 tumors 50 to 100 mm^3 in volume were randomized into groups of 10 to 12 mice and treated with 200 μg anti-IgG2a (clone 2A3; BioXcell), 100 μg anti-CD40 (clone FGK4.5; BioXcell), or 200 μg anti-CSF1R (clone AFS98; BioXcell) per dose. The combination group received 100 μg FGK4.5 and 200 μg AFS98 given at the same time but in separate injections on opposite sides of the abdomen (treatment was not premixed before injection). Doses were spaced four days apart for a total of three doses. $CD8^+$ T-cell depletion studies were carried out with randomized groups of mice bearing CT26 tumors, which were treated with 200 μg anti-CD8 (clone 2.43; BioXcell) or PBS intraperitoneally 24 hours before immunotherapy was initiated and concurrently with immunotherapy. Dosing began day 11 and continued every four days as described above. For MC-38 tumor studies, female C57BL/6 mice, 6 to 9 weeks old, harboring MC-38 tumors 75 to 125 mm^3 in volume were randomized and treated identically to the CT26 studies.

Tumor and tissue processing

Tumors were excised and dissociated into single-cell suspensions using the Miltenyi Tumor Dissociation Kit for murine tissues (catalog no. 130-096-730) per the manufacturer's instructions. Samples were filtered and mechanically processed through 70-μm nylon filters. The following draining lymph nodes (dLN) were pooled per mouse: ipsilateral brachial, axillary, and inguinal lymph nodes. Spleens or pooled dLNs were processed through 70-μm nylon filters with syringe plungers. Samples were stained for flow cytometry the same day, and remaining suspensions were stored on ice at 4°C overnight for subsequent analyses.

Flow cytometry and antibodies

For flow cytometry profiling, 2×10^6 tumor samples or 1×10^6 lymphoid tissue samples were plated in tissue culture nontreated polystyrene round bottom 96-well plates (Corning). Viability was assessed by Live/Dead Fixable Aqua Dead Cell Stain (ThermoFisher). Antibody cocktails were assembled with the following antibodies:

Myeloid stains. FITC-CD206 (clone C068C2), PE-IL4Rα (clone I015F8), PE-CD115 (clone AFS98), PE-NOS2 (clone 5C1B52), PE-CCR7 (clone 4B12), PE-IL10R (clone 1B1.3a), PE-IL10 (clone JES3-12G8), PE-IL6 (clone MP5-20F3), PE-CD103 (clone 2E7), PerCPCy5.5-F4/80 (clone BM8), PerCPCy5.5-CD80 (clone 16-10A1), PerCPCy5.5-TNFα (clone MP6-XT22), PECy7-CD103 (clone 2E7), APC-IDO (clone 2E2/IDO1), APC-TGF/LAP (clone TW7-16B4), APC-CD86 (clone GL-1), APC-F4/80 (clone BM8), AF700-Ly6C (clone HK1.4), APCCy7-I-A:I-E (MHC II; clone M5/114.15.2), BV421-Ly6G (clone 1A8), BV421-TGFβ/LAP (clone TW7-16B4), BV605-CD24 (clone 30-F1); BV650- or BV711-CD11b (clone M1/70), BV786-CD11c (clone N418), BUV395-CD45 (clone 30-F11), and dump stain BV711 for CD90.2 (clone 53-2.1) or TCRβ (clone H57-597), Siglec-F (clone E50-2440), and γδTCR (clone V65).

Lymphoid stains. FITC-Granzyme B (clone GB11), FITC-CD8 (clone 53-6.7), PE-IFNγ (clone XMG1.2), PE–T-bet (clone 4B10), PerCPCy5.5-CD4 (clone GK1.5), PECy7-Foxp3 (clone FJK-16s), PECy7-Eomes (clone Dan11mag), APC-IFNγ (clone XMG1.2), APC–TIM-3 (clone RMT3-23 or B8.2C12), AF700-CD90.2 (clone 53-2.1), AF700-CD4 (clone GK1.5), AF700-CD44 (clone IM7), APCCy7-CD90.2 (clone 53-2.1), APCCy7-CD4 (clone GK1.5), Pacific Blue-Foxp3 (clone FJK-16s), BV605–PD-1 (clone 29F.1A12), BV650-CD4, BV711-dump, BV786-CD8, BV786-CD62L, BUV395-CD45 (clone 30-F11), and BV711 for CD11b, CD11c, CD49b (clone DX5), γδTCR, and Siglec-F. AH1-tetramer: PE-conjugated $H\text{-}2L^d$ MuLV-gp70 tetramer (SPSYVYHQF; MBL International Corporation).

All antibodies were sourced from BD Biosciences, Biolegend, R&D systems, or eBioscience. Intracellular staining was performed after cellular fixation and permeabilization using either the BD Cell Fix (catalog no. 554714) or eBioscience Transcription Factor/Foxp3 staining buffer set (catalog no. 00-5523-00) according to the manufacturer's instructions. All flow cytometry data were collected on BD Fortessa instruments and analyzed by FlowJo software v9.9.4 (TreeStar).

Ex vivo functional assays

T-cell stimulation. Tumor and lymphoid tissues were processed into single-cell suspensions, and 2×10^6 tumor samples or

1×10^6 lymphoid tissue samples were plated in tissue culture nontreated polystyrene round bottom 96-well plates (Corning). Stimulation cocktail containing BD GolgiPlug (catalog no. 555029) and BD GolgiStop (catalog no. 554724) was prepared per manufacturer's instruction (final concentration 1 μL/mL for each), with or without AH1 peptide (final concentration of 5 μg/mL). Cell stimulation cocktail (500×; catalog no. 00-4970-93; eBiosciences) served as the positive control. All conditions were incubated at 37°C for four hours.

TAM intracellular staining. Tumor suspensions were plated 2×10^6 per well with GolgiStop and GolgiPlug as stated above for four hours at 37°C. Cells were surfaced-stained, fixed, and permeabilized. Samples were then stained intracellularly for IL6, TNFα, and nitric oxide synthase 2 (NOS2, iNOS). TAMs (viable, Dump$^-$ CD11b$^+$ Ly6G$^-$ Ly6C^{lo} F4/80+) were assessed for IL6, TNFα, and NOS2.

TME cytokine measurement

The day after treatment ended, tumors were weighed and homogenized with a MP FastPrep-24 instrument at 4.5 m/s for 45 seconds. Samples were filtered, centrifuged to collect the soluble fraction, and stored at −80°C. Analytes were measured using the Meso Scale Diagnostics Biomarker Group 1 Mouse 27-plex kit (catalog no. K15069L-2; Meso Scale Diagnostics). Results were analyzed by the MSD Discovery Workbench software. Calibrators 5, 7, and 8 were used as per manufacturer's instructions and served as controls.

Statistics and graphing with GraphPad Prism v6

On all graphs, mean and standard error of the mean (SEM) are shown unless otherwise indicated. Differences between treatment groups measured at endpoint were determined using analysis of variance (ANOVA) followed by *post hoc* all-pairwise comparison tests with a Tukey adjustment for multiple comparisons. Survival analysis was performed using log-rank test. Statistical analyses were run using GraphPad Prism version 6 (GraphPad Software). Statistical significance was accepted at $P < 0.05$. All comparisons stated in results are versus isotype, unless otherwise specified.

Results

Combined anti-CD40 and CSF-1R blockade improves tumor control and survival

Tumor-infiltrating myeloid cells, including TAMs, suppress antitumor immunity, and these populations rely on CSF-1/CSF-1R signaling for survival, development, and differentiation. To determine which myeloid subsets depend on the CSF-1/CSF-1R axis, CSF-1R expression was assessed in distinct populations of myeloid cells in established, untreated CT26 tumors. We used a gating strategy previously described by Movahedi and colleagues, which uses Ly6C and MHC class II (MHC II) expression to discriminate populations in the Ly6C^{hi} and Ly6C^{lo} gates (31, 32). Specifically, in this analysis, MHC II expression distinguishes Ly6C^{hi} monocytes (Ly6C^{hi} MHC II^{lo}) from Ly6C^{int} TAMs (Ly6C^{int} MHC II^{hi}; Supplementary Fig. S1A). Ly6C^{lo} F4/80$^+$ TAMs can be separated into proinflammatory MHC II^{hi} TAMs (Ly6C^{lo} F4/80$^+$ MHC II^{hi}) and alternatively activated, suppressive MHC II^{lo} macrophages (Ly6C^{lo} F4/80$^+$ MHC II^{lo}; Supplementary Fig. S1A). Compared with isotype control staining, DCs, Ly6C^{int} MHC II^{hi} TAMs, Ly6C^{lo} MHC II^{hi}, and MHC II^{lo} TAMs demonstrated increased surface expression of CSF-1R, whereas Ly6G$^+$ neutrophils maintained lower expression (Supplementary Fig. S1B). The highest frequencies of CSF-1R^{hi} cells were detected in Ly6G^{lo} Ly6C^{int} MHC II^{hi} and Ly6C^{lo} TAMs, with no significant differences in CSF-1R expression between MHC II^{hi} or MHC II^{lo} TAMs (Supplementary Fig. S1B). Together, these expression profiles correlate with data in the literature and suggest mature TAMs would be sensitive to CSF-1R blockade.

We hypothesized that blocking the CSF-1/CSF-1R pathway in CT26 tumors would result in significant changes in TAMs, and that coupling CSF-1R inhibition with CD40 agonism would result in enhanced antitumor activity. Anti–CSF-1R monotherapy failed to significantly control CT26 tumor burden compared with isotype control, whereas anti-CD40 agonist treatment delayed tumor growth (Fig. 1). Treatment with the combination resulted in the most significant control of tumor growth and extended survival (Fig. 1A–C and E). Similar results were seen in MC-38 tumors. Combination anti-CD40/anti–CSF-1R treatment elicited superior control of tumor growth compared with isotype or monotherapy-treated groups. As in CT26 studies, anti–CSF-1R monotherapy treatment failed to limit MC-38 tumor burden, whereas anti-CD40 monotherapy significantly controlled progression but not to the extent of combination treatment (Fig. 1F and G). Although these therapies targeted myeloid cells that expressed CD40 and CSF-1R, depletion of CD8$^+$ T cells in the CT26 model abrogated the antitumor efficacy of anti-CD40 monotherapy and combination treatment, as well as eliminated survival benefits observed with combination treatment (Fig. 1C–E), suggesting adaptive immune responses are critical for these responses.

Combination immunotherapy results in reduced TAMs and alters myeloid populations

To understand mechanisms underlying the improved efficacy and survival mediated by anti-CD40 and anti–CSF-1R therapy, we profiled the immune composition of tumors harvested at two time points during treatment: 24 hours after the first dose and 24 hours after the final dose. At both time points, groups that received anti-CD40 or combination anti-CD40/anti–CSF-1R exhibited similar frequencies of CD45$^+$ hematopoietic cells compared with isotype controls. However, tumors treated with anti–CSF-1R monotherapy contained approximately 10% fewer CD45$^+$ cells (Supplementary Fig. S2A). No changes were observed in the frequencies of CD11b$^+$ cells, targeted by anti-CD40 and anti–CSF-1R, at either time point across treatment groups (Supplementary Fig. S2B).

We used Ly6C and Ly6G expression to subdivide CD11b$^+$ populations into monocytes, macrophages, and neutrophils and identified broad changes in the immune infiltrates across groups. Combination-treated tumors exhibited the greatest reduction in Ly6G$^+$ cells, which includes neutrophils and polymorphonuclear MDSCs, and Ly6C^{lo} F4/80$^+$ TAMs (Fig. 2A and B). In contrast, Ly6C^{hi} cells increased significantly over isotype in all treatment groups. The greatest increase was seen in combination-treated tumors, which was also significantly greater than both monotherapies (Fig. 2B).

According to this model of subset analysis, the Ly6C$^+$ fraction consists of both monocytes and Ly6C^{int} tumor–associated macrophages, but the accumulation of Ly6C^{hi} cells in combination-treated tumors was not due to proportionate increases of both cell types (Fig. 2C–E). Analysis of MHC II expression revealed a nonsignificant increase in frequencies of Ly6C^{hi} MHC II^{lo}

monocytes in monotherapy- and combination-treated tumors (Fig. 2D) and that increased Ly6C^{int} MHC II^{hi} TAMs were primarily responsible for the overall increase in Ly6C^{+} cells (Fig. 2D and E). Both monotherapies elicited increases in Ly6C^{int} macrophages within tumors as well, with anti-CD40 treatment eliciting 2-fold more Ly6C^{int} macrophages than isotype treatment (Fig. 2E). The most significant changes were found in combination-treated tumors, where 4-fold more Ly6C^{int} macrophages accumulated over the course of treatment compared with isotype controls and were significantly higher than both monotherapies (Fig. 2E).

Approximately 70% of CD11b^{+} Ly6G^{-} myeloid-lineage cells in isotype-treated tumors consisted of Ly6C^{lo} TAMs, which were detected in both MHC II^{hi} and MHC II^{lo} populations (Fig. 2C, F and G). All treatment approaches decreased frequencies of MHC II^{lo} TAMs compared with the isotype group, with the fewest MHC II^{lo} TAMs detected after combination treatment (Fig. 2C and F). Relative to isotype controls, we observed a 33%, 50%, and 70% reduction in MHC II^{lo} suppressive TAMs in anti–CSF-1R, anti-CD40, and combination-treated groups, respectively (Fig. 2F). Frequencies of MHC II^{hi} TAMs in monotherapy groups were not significantly different from isotype-treated groups, whereas nearly half of MHC II^{hi} TAMs were reduced with combination treatment (Fig. 2G). Together, these data indicate that anti–CSF-1R and CD40 agonism differentially affect TAM and monocyte populations and that anti-CD40/anti–CSF-1R combination treatment significantly skews the composition of tumor-infiltrating CD11b^{+} myeloid cells.

CD40 agonism or combination immunotherapy increases proinflammatory TAMs

Low frequencies of Ly6C^{lo} TAM subsets led us to investigate the polarization status of the total Ly6C^{lo} F4/80^{+} TAM population. We first assessed expression of cell-surface markers associated with inflammatory MHC II^{hi} TAMs and alternatively activated MHC II^{lo} macrophages on total Ly6C^{lo} F4/80^{+} TAMs after treatment concluded. Typically, alternatively activated TAMs have high expression of IL4Rα, MMR (CD206), MerTK, and IL10R, consistent with MHC II^{lo} TAM sensitivity to suppressive signals. TAMs from tumors treated with anti-CD40 or combination anti-CD40/anti–CSF-1R exhibited decreased expression of IL4Rα, IL10R, and CD206 compared with anti-CSF-1R and isotype groups (Fig. 3A–D). Expression of inhibitory ligands, PD-L1 and PD-L2, did not change significantly across treatment groups in the majority of the experiments performed (Fig. 3E and F). In contrast, TAMs in anti-CD40 and combination-treated tumors expressed markers consistent with activation (CD83) and maturation (CD80 and CD86) of proinflammatory MHC II^{hi} macrophages (Fig. 3G–I), with highest expression observed in anti-CD40 and combination-treated groups, consistent with CD40 ligation-induced activation (ref. 33; Fig. 3G–I). Anti–CSF-1R monotherapy elicited increased expression of CD80 and CD83 markers compared with isotype controls, but did not affect activation markers in alternatively activated MHC II^{lo} TAMs. These data suggest that combination treatment aids polarization of remaining TAM

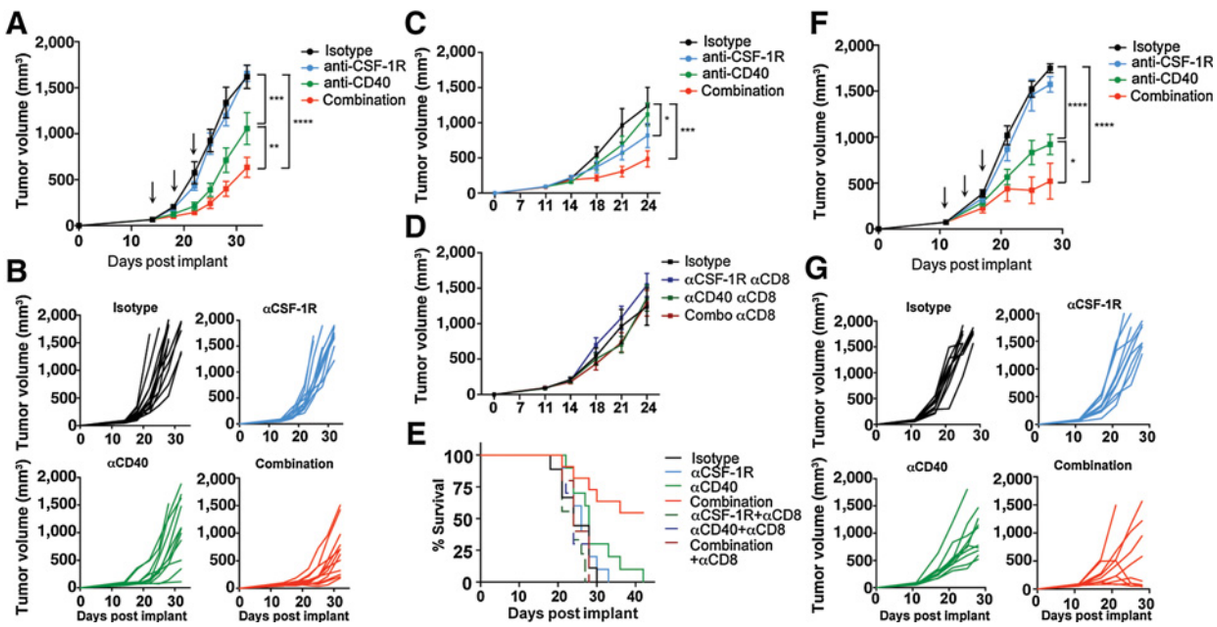

Figure 1.

Combination immunotherapy with α CD40 agonist and CSF-1R blockade controls tumor burden. **A,** Tumor volumes over time of Balb/c mice implanted with CT26 at day 0. Dates of treatment indicated by arrows. *, $P < 0.05$; **, $P < 0.005$; ***, $P < 0.0003$; ****, $P < 0.0001$. **B,** Individual tumor volume traces per mouse. $n = 12$ per group. Data are representative of four independent experiments. **C** and **D,** Tumor volumes of Balb/c mice implanted with CT26 tumors with and without CD8^{+} T cell depletion. **C,** Isotype-control antibody (intact CD8^{+} T cells) and **D,** anti-CD8 antibody. Data are representative of two independent experiments. **E,** Kaplan–Meier analysis of survival. Pairwise comparison of tumor growth with anti-CD40 or combination treatment $P = 0.011$. **F,** Tumor volumes of C57BL/6 mice implanted with MC-38 at day 0. Dates of treatment indicated by arrows. *, $P < 0.05$; **, $P < 0.005$; ***, $P < 0.0003$; ****, $P < 0.0001$. **G,** Individual tumor volume traces per mouse. $n = 10$ per group. **F** and **G,** Data are representative of three independent experiments. **A–G**, Isotype (white), anti–CSF-1R (blue), anti-CD40 (green), and combination (red). Significance between treatment groups measured at endpoint was determined using ANOVA followed by *post hoc* all-pairwise comparison tests with a Tukey adjustment for multiple comparisons.

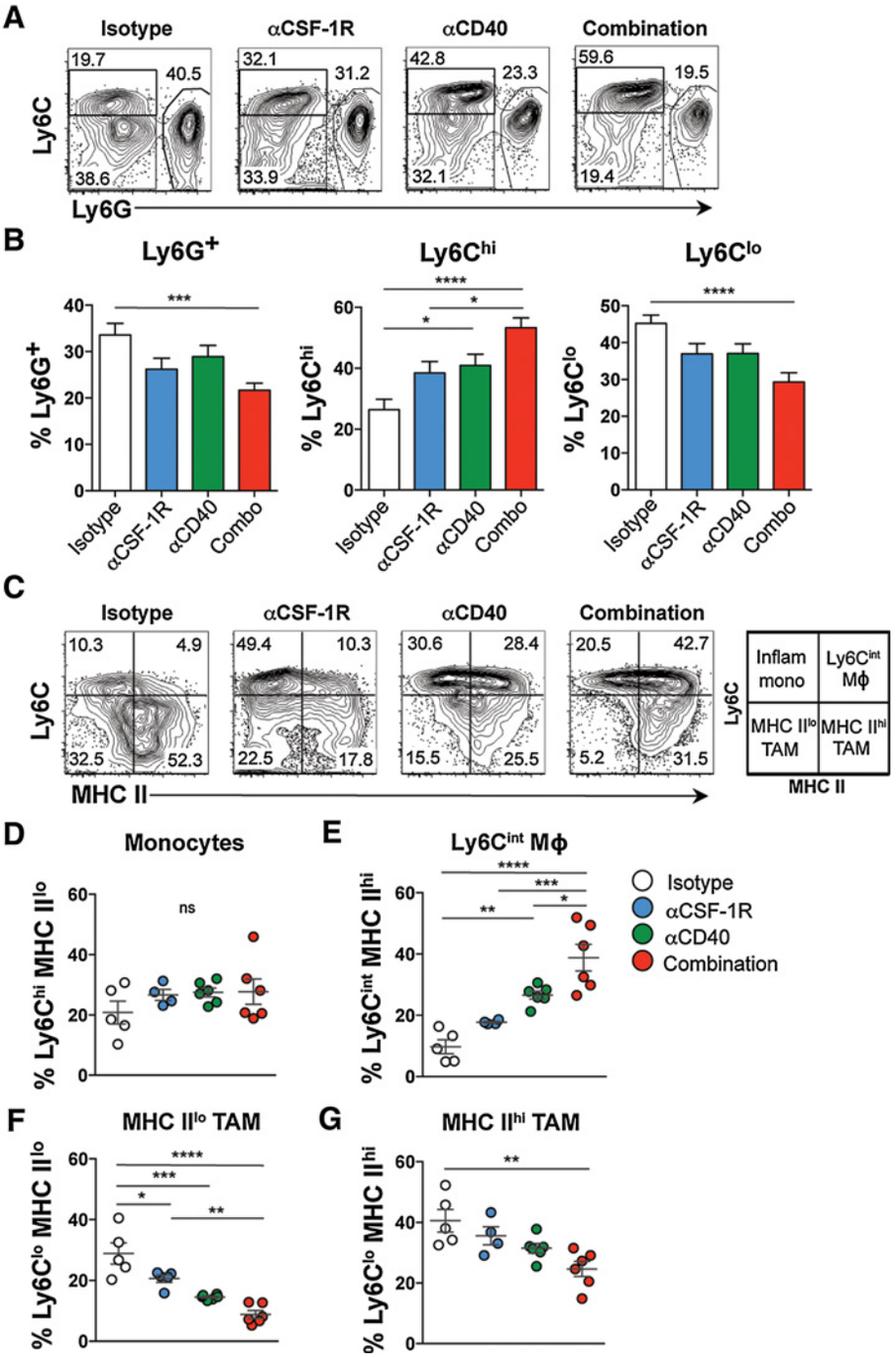

Figure 2.

CD40 and combination immunotherapy skews the composition of monocyte and macrophage populations. **A,** Representative plots of monocytes, macrophages, and neutrophils. Events are gated on live, singlet, size- and lineage-excluded CD45$^+$ CD11b$^+$ tumor-infiltrating cells. **B,** Frequency of Ly6G$^+$, Ly6C^{hi} Ly6G$^-$, or Ly6C^{lo} Ly6G$^-$ cells. Compiled from four independent experiments. $n \geq 15$ for each group. *, $P < 0.05$; **, $P < 0.01$; ***, $P < 0.005$; ****, $P < 0.0005$. **C,** Representative plots of monocytes, Ly6C^{int} macrophages, and TAMs. Populations depicted correlate with the schematic (far right). **D–G,** Compiled frequencies of indicated populations across groups. $n \geq 5$. *, $P < 0.05$; **, $P \leq 0.003$; ***, $P \leq 0.0006$; ****, $P < 0.0001$. (**A–G**) isotype (white), anti–CSF-1R (blue), anti-CD40 (green), combination (red). Significance between treatment groups measured at endpoint was determined using ANOVA followed by *post hoc* all-pairwise comparison tests with a Tukey adjustment for multiple comparisons. Data are representative of three experiments.

populations from the MHC II^{lo} suppressive TAM phenotype toward MHC II^{hi} proinflammatory TAMs.

Based on expression of markers affiliated with proinflammatory TAMs, we hypothesized that macrophages from anti-CD40 and combination anti–CD40/anti–CSF-1R would be primed to generate proinflammatory signals. Anti-CD40 and anti-CD40/anti–CSF-1R treatment induced increased frequencies of TNFα$^+$ and NOS2$^+$ TAMs compared with isotype- or anti–CSF-1R-treated groups (Fig. 3J–L). Latency-associated protein (LAP) was evaluated as a surrogate for the immunosuppressive cytokine TGFβ. Anti-CD40 and combination treatment decreased the fraction of TAMs poised to produce TGFβ in tumors, whereas anti–CSF-1R monotherapy was not appreciably different from isotype treatment (Fig. 3M).

IL10/IL10R signaling is associated with suppression of antitumor immune responses (34, 35). Reduced frequencies of IL10-producing TAMs were observed in all treated groups compared with isotype controls (Fig. 3N), with only the combination-

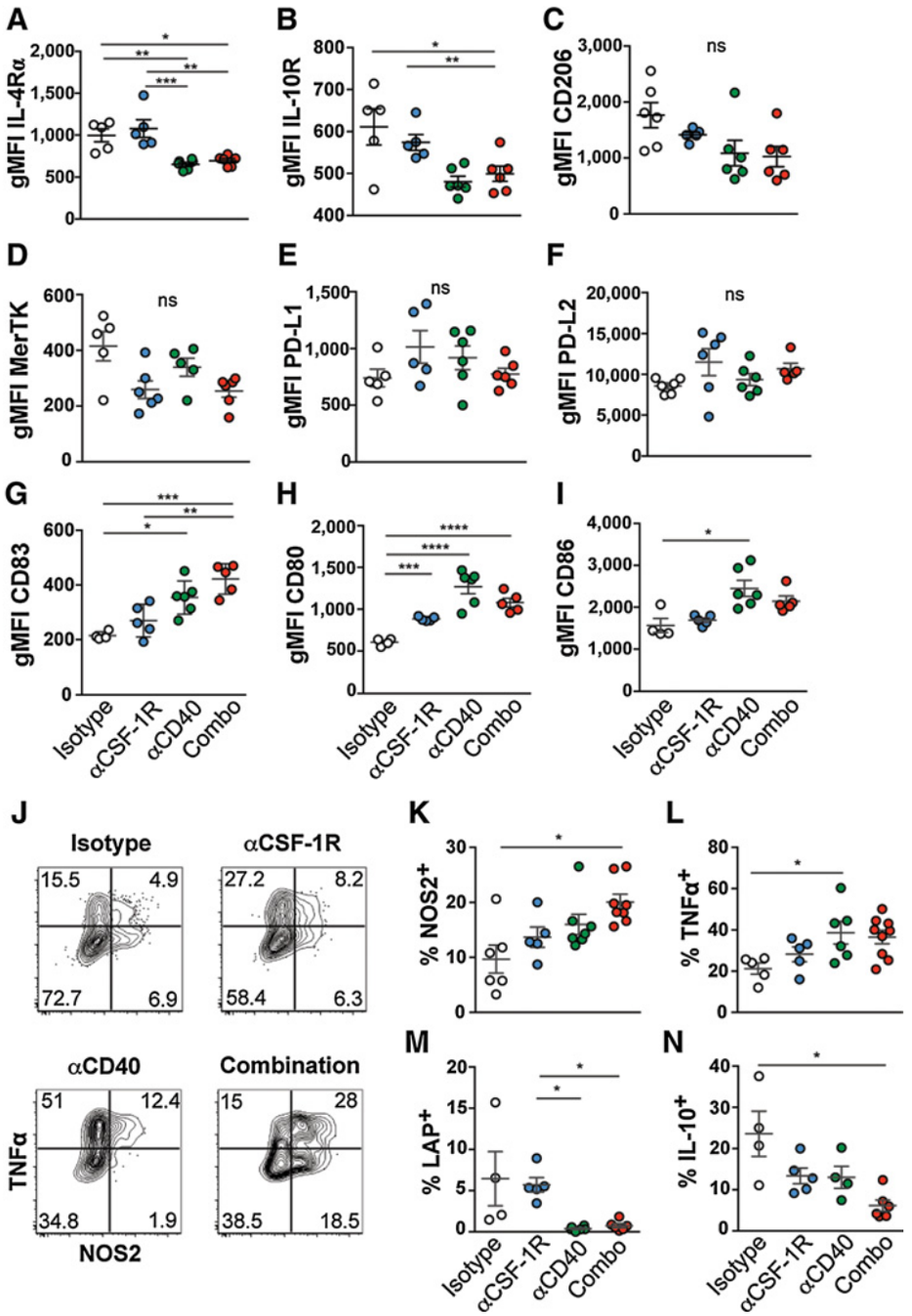

Figure 3.

Combination therapy promotes a proinflammatory phenotype in remaining TAMs. **A–I,** Geometric mean fluorescent intensity (gMFI) of total TAMs ($CD11b^+$ $Ly6G^-$ $Ly6C^{lo}$ $F4/80^+$) from tumors harvested after treatment regimen. gMFI of (**A**) IL4Rα, (**B**) IL10R, (**C**) CD206, (**D**) MerTK, (**E**) PD-L1, (**F**) PD-L2, (**G**) CD83, (**H**) CD80, and (**I**) CD86 on TAMs. *, $P < 0.05$; **, $P \leq 0.003$; ***, $P \leq 0.0006$; ****, $P < 0.0001$. **J,** Intracellular staining for cytokine or effector molecules TNFα and NOS2. Relative frequencies of TAMs stained for (**K**) NOS2, (**L**) TNFα, (**M**) LAP (pro-TGFβ), and (**N**) IL10. **A–N**, Isotype (white), anti–CSF-1R (blue), anti-CD40 (green), combination (red). Significance between treatment groups measured at endpoint were determined using ANOVA followed by *post hoc* all-pairwise comparison tests with a Tukey adjustment for multiple comparisons. Data are representative of three experiments.

treated group reaching significance. Therefore, combination treatment reduced levels of LAP/TGFβ, IL10, and IL10R in suppressive TAM populations, increased frequencies of activated MHC II^{hi} macrophages, and skewed the TME toward a proinflammatory phenotype.

Combination therapy induces accumulation of activated $CD103^+$ DCs in dLNs

Efficient antigen presentation by DCs is critical to priming effective antitumor T-cell responses, and CD40 agonism is known to drive DC activation and maturation (36, 37). In anti-CD40 or anti–CD40/anti-CSF-1R-treated tumors harvested after the end of treatment, CD83, CD80, and CD86 expression was increased on intratumoral DCs compared with isotype-treated DCs, whereas anti–CSF-1R monotherapy did not significantly change the activation status of these APCs (Fig. 4E). Lower frequencies of DCs ($CD24^{hi}$ MHC II^{hi} $CD11c^+$) were observed in tumors from anti-CD40 and combination-treated groups compared with isotype controls 24 hours after start of treatment (Fig. 4A). We hypothesized that DCs could be trafficking to lymphoid tissues after activation via CD40 agonism and, therefore, examined dLNs 24 hours after the initial dose. Consistent with our hypothesis,

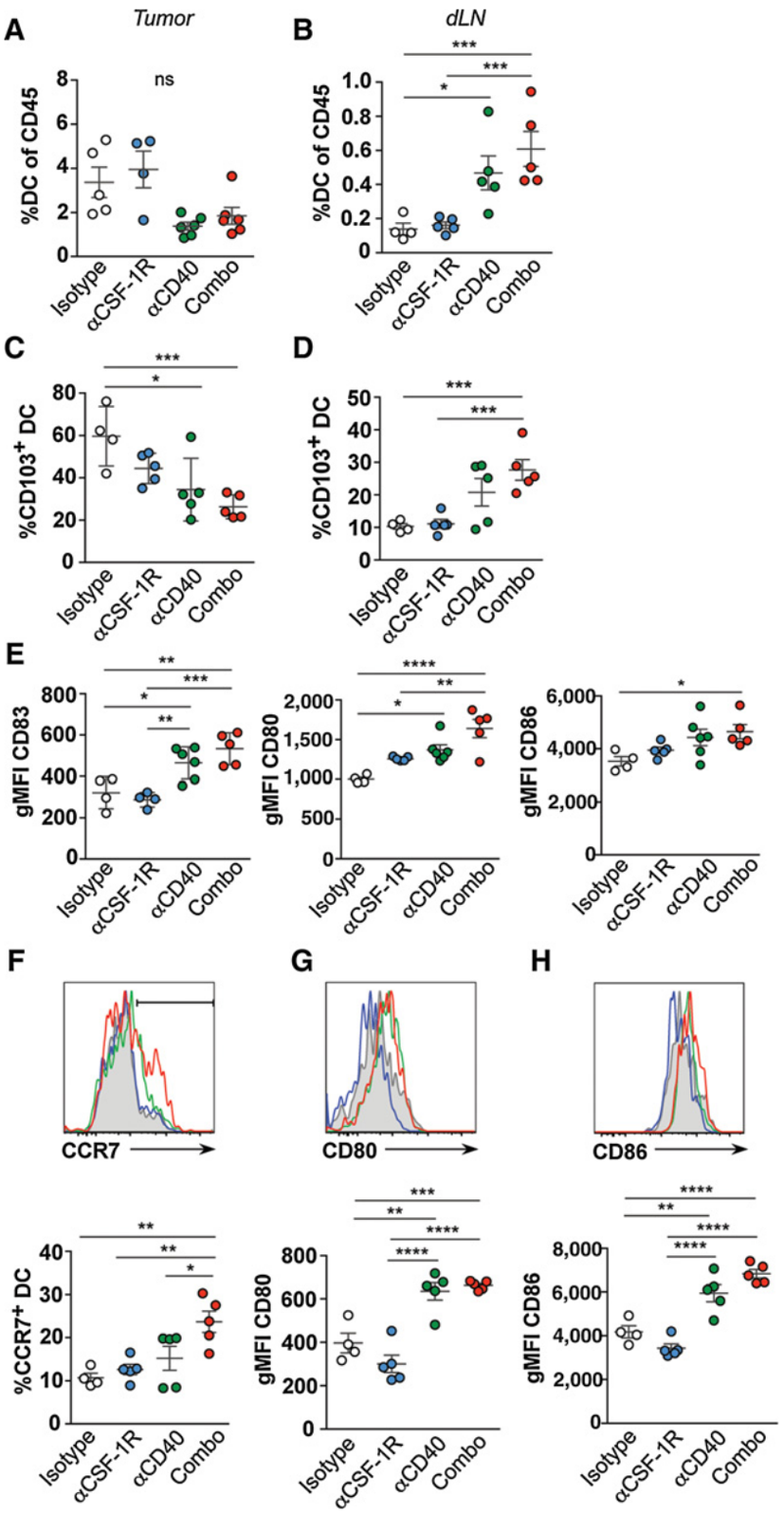

Figure 4.

In dLNs, CD103$^+$ DCs express increased markers of activation and accumulate in dLN after one dose. Twenty-four hours after initial dosing, mice were sacrificed and tumors and dLNs were harvested. **A** and **B,** Frequency of DCs (CD24^{hi} MHC II^{hi} CD11c$^+$) of total CD45$^+$ infiltrates in (**A**) tumors or (**B**) dLNs. **C** and **D,** Frequency of CD103$^+$ DCs of total DCs in (**C**) tumor or (**D**) dLNs. **E,** Expression of activation markers on intratumoral DCs at the conclusion of treatment. **F–H,** Expression of activation markers on DCs in the dLNs from animals treated with isotype (gray filled histogram), anti–CSF-1R (blue line), anti-CD40 (green line), or combination (red line). **F,** CCR7 expression and compiled frequencies of CCR7$^+$ DC in dLNs. **G** and **H,** Expression and compiled gMFI of (**G**) CD80 or (**H**) CD86 on DC in dLNs. (**A–H**) *, $P < 0.05$; **, $P < 0.01$; ***, $P < 0.0005$; ****, $P < 0.0001$. (**A–H**) isotype (white), anti–CSF-1R (blue), anti-CD40 (green), combination (red). Significance between treatment groups measured at endpoint was determined using ANOVA followed by *post hoc* all-pairwise comparison tests with a Tukey adjustment for multiple comparisons. Data are representative of four experiments.

significant DC accumulation was observed in the dLNs of animals treated with anti-CD40 or combination therapy but not isotype or anti–CSF-1R monotherapy (Fig. 4B).

CD103 expression marks a subset of nonlymphoid classical DCs that have been implicated in cross presentation of tumor antigens and T-cell priming in lymphoid tissues (38, 39). $CD103^+$ DCs were reduced in tumors one day after anti-CD40 or combination treatment began but made up a significant fraction of total DCs in matched dLNs at the same time point (Fig. 4C and D). A higher proportion of these DCs in the dLNs expressed markers of migration and maturation: CCR7, CD83, CD80, and CD86 (Fig. 4F–H). Together, these findings demonstrate anti-CD40 agonism with CSF-1R blockade drives accelerated maturation and sustained activation of DCs and macrophages in tumors and increased frequencies of mature DCs in draining lymph nodes.

Enhanced $CD8^+$ T-cell effector function in the dLNs of combination-treated mice

Although the individual treatments in this combination approach targeted myeloid cells, control of tumor growth by anti-CD40/anti-CSF-1R therapy was mitigated when $CD8^+$ T cells were depleted *in vivo*. Therefore, adaptive immune responses are critical for tumor rejection mediated by anti-CD40/anti-CSF-1R therapy. Given the increased accumulation and activation of DCs in the dLNs of anti-CD40 and anti-CD40/anti–CSF-1R-treated mice, we next investigated whether T cells in dLNs and tumors mounted improved antitumor effector responses. After treatment concluded, increased frequencies of $CD8^+$ T cells were detected in the dLNs of anti-CD40 and anti-CD40/anti–CSF-1R-treated animals but not after anti–CSF-1R treatment alone (Fig. 5A).

Because $CD103^+$ DCs are capable of trafficking tumor antigen to dLNs (38) and increased $CD103^+$ DCs were found in the dLNs of combination-treated animals, we sought to evaluate tumor antigen–specific $CD8^+$ T-cell responses in dLNs. CT26 tumor cells express AH1 peptide, which is found in an envelope glycoprotein (gp70) of murine leukemia virus. Tetramer staining revealed an increased frequency of AH1-specific $CD8^+$ T cells in the dLNs of anti-CD40/anti–CSF-1R-treated mice after treatment concluded (Fig. 5B), indicating that combination treatment expanded the tumor AH1-specific T cells.

Responses against AH1 serve as a surrogate measurement of tumor antigen–specific $CD8^+$ T-cell activity. To assess T-cell function, $CD8^+$ T cells from dLNs were rechallenged with AH1 peptide *ex vivo*. Only $CD44^{hi}$ effector $CD8^+$ T cells from combination-treated mice, but not from either monotherapy, exhibited improved T-cell function on rechallenge (Fig. 5C–F). Significantly higher frequencies of $IFN\gamma^+$ $CD44^{hi}$ or $TNF\alpha^+$ $CD44^{hi}$ $CD8^+$ T cells were found in the dLNs of combination-treated animals compared with monotherapy or isotype groups (Fig. 5C–F).

Along with increased effector function, $CD8^+$ T cells also demonstrated increased expression of activation markers and upregulation of checkpoint molecules PD-1, TIM-3, LAG-3, and TIGIT (Supplementary Fig. S3A and S3B). Patterns of increased PD-1 and TIM-3 coexpression on $CD8^+$ T cells were similar in anti-CD40 and anti-CD40/anti-CSF-1R-treated groups, whereas <1% of $CD8^+$ T cells expressed either PD-1 or TIM-3 in the dLNs of anti–CSF-1R- or isotype-treated groups. $CD8^+$ T cells from anti-CD40 or combination-treated animals expressed multiple checkpoint markers, whereas <3% of $CD8^+$ T cells expressed more than one of these receptors after anti–CSF-1R or isotype treatment (Supplementary Fig. S3B). More $CD8^+$ T cells from the dLNs of combination-treated animals exhibited an activated cell-surface phenotype and increased expression of the T-box transcription factor (T-bet) and Eomesodermin (Eomes), two transcription factors critical for effector function (Supplementary Fig. S3C–S3F). Anti-CD40 treatment was sufficient to drive increased expression of these transcription factors relative to isotype and anti–CSF-1R-treated groups but not to the extent observed in combination-treated groups. Taken together, anti-CD40/anti–CSF-1R treatment triggers enhanced APC priming resulting in expanded antigen-specific effector $CD8^+$ T cells in dLNs.

Combined immunotherapy increased $CD8^+$ TILs and enhanced $CD8^+$ effector responses

We next investigated how improved antigen responses in dLNs of treated animals correlated to effector lymphocyte responses in tumors. First, we assessed frequencies of total T cells of $CD45^+$ infiltrating immune cells in tumors. After treatment concluded, anti–CD40/anti-CSF-1R tumors contained more T cells on average than isotype-treated tumors, whereas anti–CSF-1R and anti-CD40 monotherapies drove smaller but reproducible increases in T-cell frequencies (Fig. 5G). Within the $Thy1^+$ fraction, $CD8^+$ TIL frequencies were significantly increased across all treatment groups compared with isotype-treated tumors, with the most significant increase detected in the anti-CD40/anti–CSF-1R group that exhibited almost 40% more $CD8^+$ TILs compared with isotype controls (Fig. 5H). Increased $Thy1^+$ and $CD8^+$ T cells resulted in increased $CD8^+$ T cells within the total $CD45^+$ immune infiltrate in tumors treated with anti-CD40/anti–CSF-1R therapy (Supplementary Fig. S2C). Moreover, the absolute number of $CD8^+$ T cells was increased per gram of tumor after combination or anti-CD40 treatment (Supplementary Fig. S2F). These data demonstrate that more $CD8^+$ T cells infiltrate tumors after CD40 agonism or CSF-1R blockade, but the combination is more effective than either monotherapy. However, unlike the findings in dLNs, the proportion of AH1 $tetramer^+$ $CD8^+$ cells was not significantly altered in tumors across treatment groups (Fig. 5I).

To determine whether intratumoral T-cell effector responses improved with combination immunotherapy, we assessed the phenotype and function of $CD8^+$ TILs in CT26 tumors by measuring expression of activation markers in total $CD8^+$ TILs and AH1 $tetramer^+$ $CD8^+$ T cells. Similar to $CD8^+$ T cells in dLNs, activation markers and checkpoint molecules, PD-1, TIM-3, TIGIT, and LAG-3, were increased on $CD8^+$ TILs after anti-CD40 or combination immunotherapy, relative to isotype-treated tumors (Supplementary Fig. S3G and S3H). Combination treatment led to increased frequencies of $CD8^+$ TILs coexpressing PD-1 and TIM-3, and nearly half of $CD8^+$ TILs coexpressed multiple checkpoint molecules, indicating enhanced effector activation (Supplementary Fig. S3H).

Restimulation with AH1 peptide *ex vivo* revealed that anti-CD40/anti–CSF-1R combination immunotherapy elicited significantly higher frequencies of antigen-specific $CD8^+$ TILs primed to produce IFNγ, TNFα, or granzyme B in response to tumor antigen (Fig. 5J). A higher proportion of $CD8^+$ TILs from combination-treated tumors were also able to mount polyfunctional responses in response to AH1 peptide (Fig. 5J). Together, these data suggest that anti-CD40/anti–CSF-1R immunotherapy enhances both the quality and quantity of $CD8^+$ TILs.

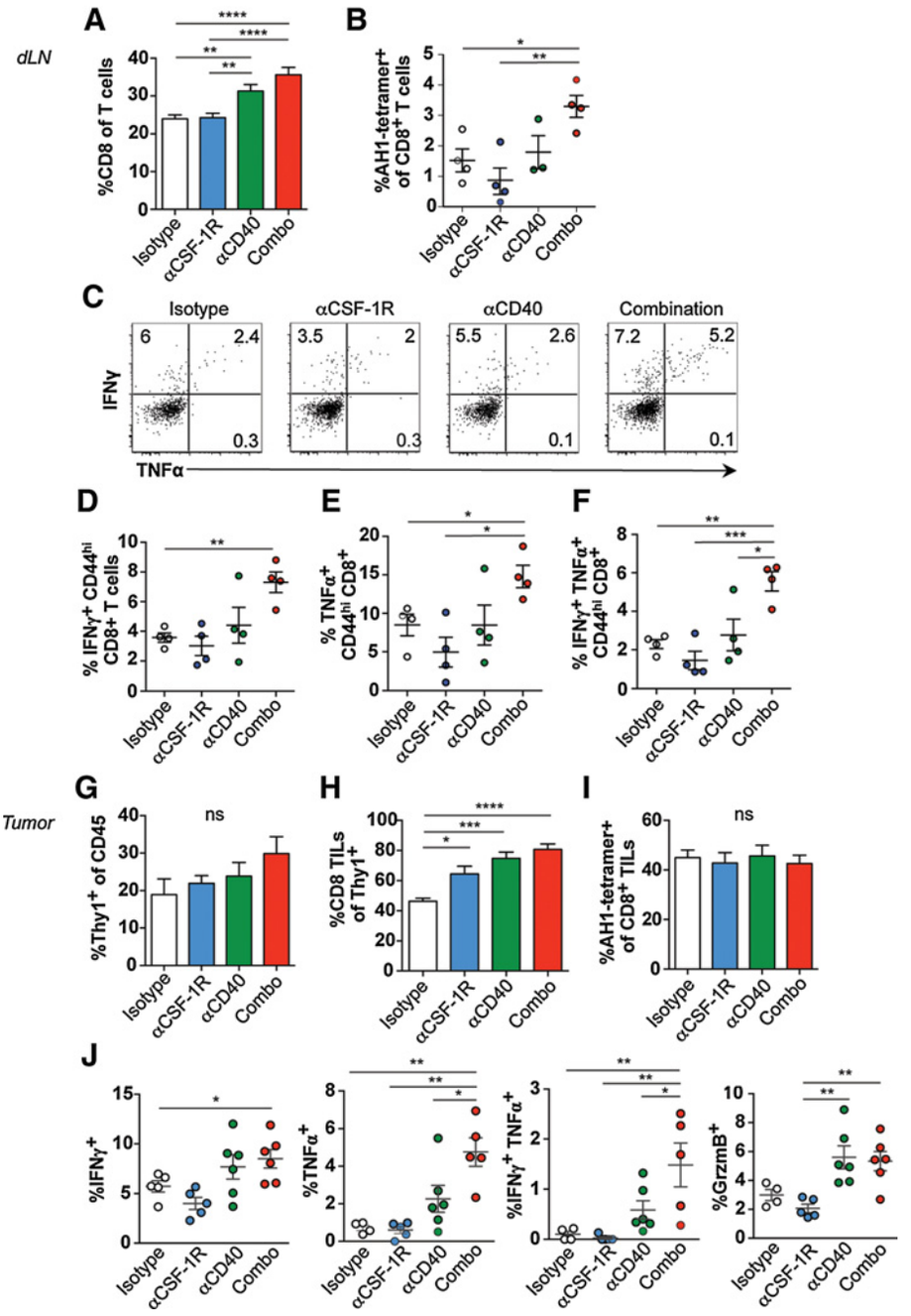

Figure 5.

Combination immunotherapy improved tumor antigen–specific responses in dLNs and tumors. After treatment concluded, tumors were harvested and dLNs were pooled per animal. **A,** Frequency of $CD8^+$ T cells in dLNs compiled from three independent experiments. $n \geq 12$ for each group. **B,** Frequency of AH1 $tetramer^+$ $CD8^+$ T cells in dLNs. **C,** Intracellular staining for IFNγ and TNFα after rechallenge *ex vivo* with AH1 peptide. Numbers within gates represent relative frequencies of total $CD44^{hi}$ $CD8^+$ T cells from dLNs. **D–F,** Frequencies of $CD44^{hi}$ $CD8^+$ T cells in dLNs that produced (**D**) IFNγ, (**E**) TNFα, or (**F**) IFNγ and TNFα in response to AH1 peptide rechallenge. **A–F**: *, $P < 0.05$; **, $P < 0.01$; ***, $P < 0.005$; ****, $P < 0.0005$. Significance was determined using ANOVA followed by *post hoc* all-pairwise comparison tests with a Tukey adjustment for multiple comparisons. Representative of four independent experiments. **G,** Compiled frequency of $Thy1^+$ cells of total $CD45^+$ immune infiltrates in tumors. $n \geq 13$ for each group. **H,** Compiled frequencies of $CD8^+$ T cells in tumors of $Thy1^+$ events. $n \geq 13$ for each group. **I,** Compiled frequency of AH1-tetramer antigen-specific $CD8^+$ T cells of total $Thy1^+$ $dump^-$ events in tumors. $n \geq 22$ per group. **J,** Compiled frequencies of $IFN\gamma^+$, $TNF\alpha^+$, or $IFN\gamma^+$ $TNF\alpha^+$, or Granzyme B^+ $CD8^+$ TILs after rechallenge with AH1 peptide. **G–J**: *, $P < 0.05$; **, $P \leq 0.01$; ***, $P \leq 0.001$; ****, $P < 0.0001$. **A–J**, Isotype (white), anti–CSF-1R (blue), anti-CD40 (green), combination (red). Significance was determined using ANOVA followed by *post hoc* all-pairwise comparison tests with a Tukey adjustment for multiple comparisons. **G–I**, Data are compiled from three studies. **J,** Data are representative of four experiments.

Tumor-infiltrating regulatory T cells are decreased in tumors with combination treatment

Anti-CD40/anti–CSF-1R treatment resulted in increased frequencies and improved function of $CD8^+$ TILs, as well as decreased frequencies of $Foxp3^-$ conventional $CD4^+$ TILs. Although frequencies of $CD4^+$ T cells were decreased in the immune infiltrate of anti-CD40 or combination-treated tumors, the number of helper T cells per gram of tumor was increased, reflecting overall increased immune infiltration induced by anti-CD40 or combination treatment (Supplementary Fig. S2F). Additionally, the remaining helper $CD4^+$ $Foxp3^-$ T cells in both dLNs and tumors treated with anti-CD40/anti–CSF-1R exhibited significantly increased activation and effector function. After treatment concluded, more $CD4^+$ T cells in combination-treated animals produced IFNγ, TNFα, and IL2 in unstimulated *ex vivo* cultures (Fig. 6A and B). Anti–CSF-1R monotherapy had a role in driving improved $CD4^+$ helper responses compared with isotype controls (Fig. 6B).

Previous reports described decreased immunosuppressive $Foxp3^+$ Tregs in tumor models after either anti–CSF-1R or anti-CD40 treatment (40, 41). We assessed whether similar changes were observed in this subset of $CD4^+$ T cells after

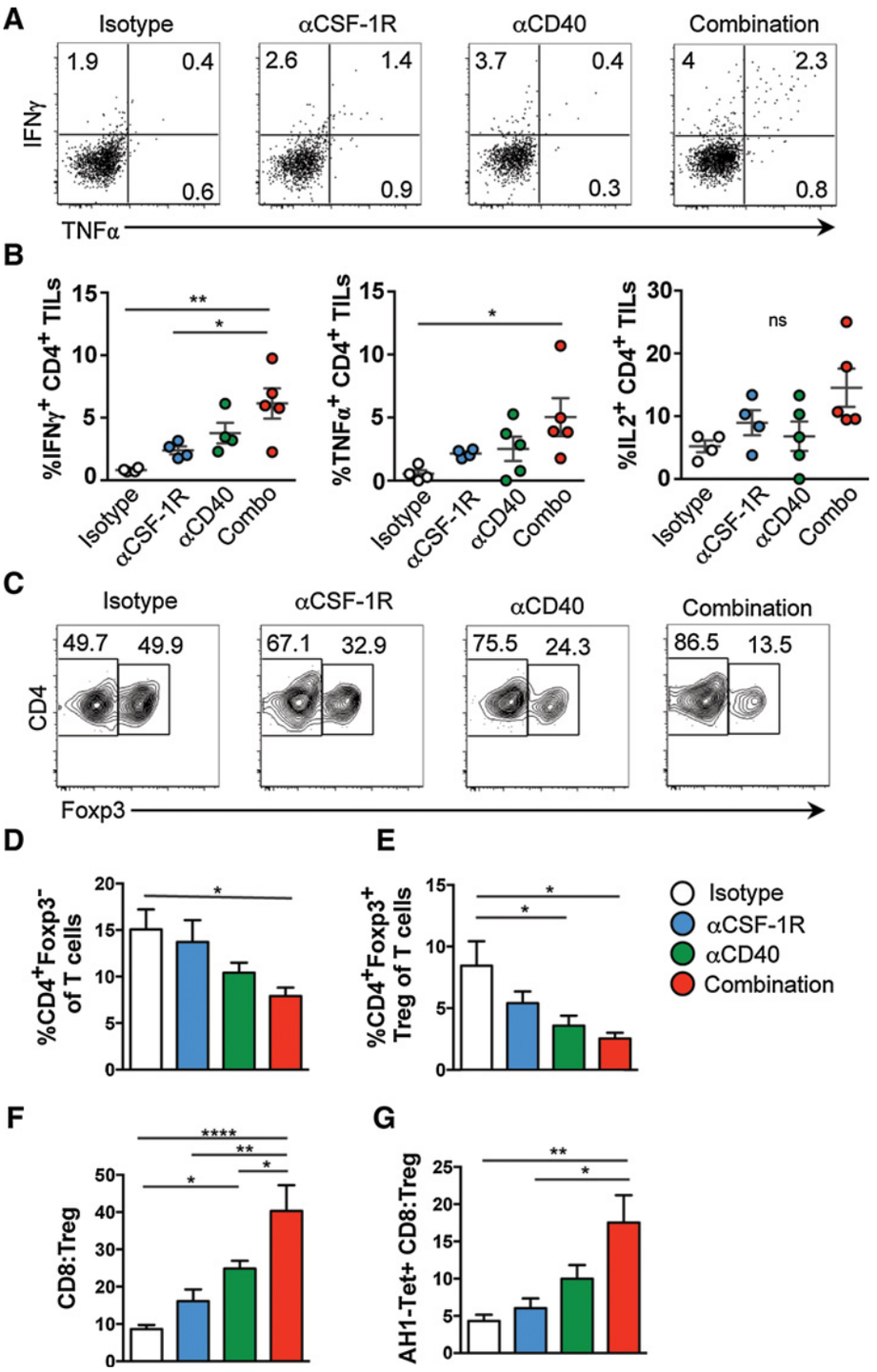

Figure 6.

Combination treatment increases activation of tumor-infiltrating $CD4^+$ helper T cells and significantly reduces $Foxp3^+$ Tregs. After treatment concluded, tumors were analyzed for changes in $CD4^+$ TILs. **A,** Representative plots of intracellular staining for IFNγ and TNFα by unstimulated $CD4^+$ $Foxp3^-$ TILs. Numbers within gates represent relative frequencies of total $CD4^+$ $Foxp3^-$ TILs. **B,** Frequencies of $CD4^+$ $Foxp3^-$ helper TILs that produced (left) IFNγ, (center) TNFα, or (right) IL2 at baseline. **C,** Representative plots of $Foxp3^-$ T cells and $Foxp3^+$ Tregs in $CD4^+$ TILs. Numbers indicate relative frequency of gated events of total $CD4^+$ TILs. **A–C,** Data are representative of four independent experiments. **D–G,** Results compiled from three independent experiments $n \geq 15$. Frequency of (**D**) $CD4^+$ $Foxp3^-$ T-helper TILs or (**E**) $CD4^+$ $Foxp3^+$ TILs of intratumoral T cells. **F,** Ratio of $CD8^+$ TILs to Tregs in tumors. **G,** Ratio of AH1 tetramer$^+$ $CD8^+$ TILs to Tregs in tumors. *, $P < 0.05$; **, $P \leq 0.01$; ***, $P \leq 0.001$; ****, $P < 0.0001$. **A–G**, Significance between treatment groups measured at endpoint was determined using ANOVA followed by *post hoc* all-pairwise comparison tests with a Tukey adjustment for multiple comparisons.

anti-CD40/anti–CSF-1R treatment. Consistent with published data, tumors treated with either anti–CSF-1R or anti-CD40 monotherapy consistently exhibited decreased frequencies of $CD4^+$ $Foxp3^+$ Tregs of total lymphocytes or total $CD45^+$ immune cells after treatment concluded (Fig. 6C and E; Supplementary Fig. S2E), and the most dramatic decrease was seen after anti-CD40/anti–CSF-1R combination treatment, which had a higher ratio of helper CD4+ T cells to T regs in combination-treated animals. A 4-fold higher ratio of $CD8^+$ TILs to Tregs was seen in combination-treated tumors compared with isotype controls (Fig. 6F). Although frequencies of AH1 tetramer$^+$ $CD8^+$ TILs did not significantly change, combination treatment resulted in a

significantly higher ratio of AH1-specific $CD8^+$ TILs to Tregs (Fig. 6G). Together, these data suggest that helper $CD4^+$ TILs and effector $CD8^+$ TILs may be able to sustain improved antitumor functions due to the decreased Treg frequency in the TME.

The cytokine milieu is more inflammatory with combination treatment

Changes we observed in both myeloid and lymphoid populations demonstrate that anti-CD40/anti-CSF-1R immunotherapy resulted in significant alterations to the immune infiltrate in CT26 tumors. To determine the sum effect of the observed changes on the TME cytokine milieu, we measured cytokine analytes in homogenized tumors and normalized analyte concentration per gram of tumor harvested. Proinflammatory cytokines TNFα, IFNγ, IL6, IL23, and IL12 were increased in tumors that received anti-CD40 or combination immunotherapy (Supplementary Fig. S4A). In anti-CD40 or combination-treated tumors, increased GM-CSF was also observed, which supports MHC II^{hi} TAM polarization. In contrast, levels of immunosuppressive cytokine IL10 were decreased in all treatment groups compared with isotype-treated tumors, including anti-CSF-1R treatment alone (Supplementary Fig. S4B). Mean levels of IL4 were also reduced ∼30% in anti-CD40 and combination-treated tumors compared with isotype controls, but the amount of IL4 was relatively minimal in all groups (Supplementary Fig. S4B). These data suggest that the total effect of combination treatment skewed the TME toward increased inflammatory cytokine production and reduced suppressive signals. Together, the phenotype and functional analysis of TAMs, monocytes, DCs, and tumor-infiltrating T cells demonstrates that anti-CD40/anti–CSF-1R immunotherapy drives a cumulative polarization of the TME toward an antitumor, proinflammatory environment, resulting in improved immune responses, overall enhanced antitumor efficacy, and extended survival.

Discussion

In this report, we investigated the efficacy of combining CD40 agonism and CSF-1R blockade to modulate endogenous antitumor immunity and control tumor growth. We demonstrated enhanced inhibition of tumor growth and extended survival with combination treatment compared with monotherapies. The improved antitumor efficacy with anti-CD40/anti–CSF-1R therapy was characterized by significant changes to the immune infiltrate that disrupted suppressive immune mechanisms and promoted inflammatory innate and adaptive antitumor responses.

The most dramatic changes in the immune infiltrate after anti-CD40/anti–CSF-1R treatment were observed in macrophage and monocyte populations. Consistent with the highest CSF-1R expression on $Ly6C^{lo}$ TAMs, combining anti–CSF-1R inhibition and CD40 agonism resulted in significantly reduced frequencies of MHC II^{hi} and MHC II^{lo} TAMs in tumors. We observed a concomitant increase in MHC II^{hi} $Ly6C^{int}$ macrophages, which suggested that combination therapy reduced the suppressive tumor-educated TAMs, while leaving newly differentiated, proinflammatory macrophages to repopulate the TME. The remaining macrophages in tumors had higher expression of costimulatory molecules CD80 and CD86, inflammatory cytokines, and lower levels of MHC II^{lo} markers, including IL10R. IL10 signaling, through its receptor IL10R, not only drives IL10 production by $Foxp3^+$ Tregs, but also antagonizes IL1- and TNFα-induced pathways and suppresses transcription of proinflammatory genes in a wide range of immune cells (34). Since increased expression of IL-10R is associated with poor control of tumor progression, the decreased IL-10R levels observed across cell types suggest that combination therapy supports resistance to IL-10-dependent suppression. Macrophages and myeloid subsets infiltrating the TME also demonstrated upregulated costimulatory molecules that potentially propagated effector T-cell responses within the tumor. Together, these data demonstrated broad changes in the balance of suppressive and inflammatory myeloid subsets functioning in tumors and illustrated how targeting CD40 pathways, together with CSF-1R inhibition, generated potent downstream effects beyond TAM depletion.

Although anti-CD40/anti–CSF-1R therapy does not directly target T cells, it has a profound effect on boosting T-cell responses. To investigate how combination treatment affected antigen presenting cells responsible for initiating T-cell responses, we explored changes in DCs across treatment groups. We found CD40 agonism alone or in combination with anti–CSF-1R reduced frequencies of DCs in tumors but increased frequencies in dLNs. DCs exhibited an activated, mature APC phenotype with increased levels of MHC II, CD80, and CD86 in both tumor and dLNs. Studies from other groups have described $CD103^+$ DCs immune surveillance and migration through nonlymphoid tissues. Upon receiving activating signals, migratory DCs traffic from surrounding tissues to dLNs to present antigens that prime lymphocytes. Accumulation of $CD103^+$ DCs was most increased with combination therapy, which may indicate CD40 agonism improves activation of $CD103^+$ DCs residing in tissues around tumor sites, enabling them to pick up and process tumor antigens for T-cell priming. Consistent with this hypothesis, AH1-specific $CD8^+$ T-cell responses were increased in magnitude. Our observation that T cells in combination-treated mice exhibited greater levels of activation and function than those in the anti-CD40 monotherapy group indicates that skewing of the macrophage population by CSF-1R contributes to the overall antitumor response. A prominent effect of combination treatment included lower quantities of IL10. IL10 signaling in DCs potently inhibits maturation and antagonizes IL12 production, resulting in poor activation of T cells and increased promotion of Treg differentiation (34, 42). Alternatively, we hypothesized that blocking CSF-1 signals may alter the composition of DCs by reducing frequencies of suppressive tolerogenic DCs that rely on this cytokine for development and survival. Together, these direct and indirect effects of anti-CD40/anti–CSF-1R treatment may increase frequencies of mature immunogenic DCs and improve T-cell priming. Therefore, the quantity and quality of T-cell responses found in combination-treated animals could result from improved APCs that couple more efficient antigen presentation with increased expression of costimulatory molecules. Our data highlight how generating antitumor T-cell responses not only within the tumor, but also in local lymphoid tissues, may support long-lived adaptive immunity.

We found combination therapy boosted the function not only of $CD8^+$ cytotoxic T cells but also of conventional $CD4^+$ T cells. These activated helper CD4+ T cells exhibited an inflammatory Th1 differentiation profile, based on production of prototypical Th1 cytokines IFNγ and TNFα. The shift in inflammatory cytokines seen in combination-treated tumors is likely driven not only by myeloid and $CD8^+$ effector activity but also by increased Th1

effector function. CD40 ligand signaling has a critical role in preserving $CD4^+$ T cell help (37, 43). Increased $CD4^+$ helper T-cell function could be induced by enhanced antigen presentation and MHC–peptide complex stability via CD83 upregulation, costimulation with increased expression of CD80 and CD86, and IL12 production (20, 21, 37). Decreased frequencies of Tregs could also contribute to the increased magnitude of $CD4^+$ T-cell effector function in anti-CD40/anti–CSF-1R-treated tumors. Future investigation will focus on whether combination therapy directly reduces Treg numbers by stimulating Th1 differentiation or changing availability of cytokines critical for maintaining Tregs' Foxp3 expression and transcriptional programs (44). As suppressive TAMs were eradicated and more inflammatory cells infiltrated combination-treated tumors, we found lower levels of IL10 and IL4 and higher levels of IL12, IFNγ, and TNFα in tumors, which may lend to the instability of $Foxp3^+$ Treg numbers and support differentiation of Th1 $CD4^+$ T cells.

Combination therapy induced significant activation of lymphocytes, concomitant with upregulation of checkpoint receptors PD-1, TIM-3, TIGIT, and LAG-3. Although coinhibitory receptors normally contribute to contraction of immune responses following pathogen clearance, checkpoint molecules in the context of cancer and chronic infection are associated with T-cell exhaustion and immune dysfunction. A critical question emerging from these mechanistic data is how to reconcile improved antitumor efficacy with TILs that phenotypically resemble exhausted lymphocytes vulnerable to intratumoral suppressive mechanisms. T-cell exhaustion is not purely a product of expression of inhibitory receptors, but a complex, progressive syndrome that develops over time in environments with multiple obstacles, including reduced $CD4^+$ T cell help, chronic exposure to antigen, and inhibitory signaling via checkpoint ligands and suppressive cytokines (45, 46). Although coexpression of checkpoint receptors was elevated on both $CD4^+$ and $CD8^+$ T cells following combination therapy, we found that expression of checkpoint ligands, PD-L1 or PD-L2, was not significantly different in the anti-CD40/anti-CSF-1R group from isotype controls. It has also been shown that increased $CD4^+$ T cell help preserves $CD8^+$ T-cell effector functions during chronic infection or in cancer (47). Therefore, exhaustion may be avoided despite upregulation of inhibitory receptors associated with immune dysfunction in cancer. Nonetheless, given the expression of numerous checkpoint receptors on T cells, antitumor efficacy of the combination of CD40 agonism and CSF-1R blockade may be further improved by including checkpoint blockade. Checkpoint blockade has complemented TAM-directed therapies in various tumor models (48–50), and future experiments will investigate whether including anti-PD-1 checkpoint blockade in combination with anti-CD40/anti–CSF-1R combination therapy will provide additional benefits.

The present studies demonstrated the advantage of combining CD40 agonism with CSF-1R blockade to produce the most effective tumor control and extend survival. Using a rigorous flow cytometry approach that enables in-depth characterization of distinct immune subsets, we have extensively profiled the phenotypic and functional changes in tumor-associated myeloid and lymphocyte populations in response to treatment. Previous reports have described the effects of CD40 agonist or anti–CSF1R monotherapy alone in murine tumor models by using the general phenotypic markers, CD11b and Gr-1, to characterize changes in the myeloid infiltrate. Our data improved the resolution on the heterogeneous myeloid populations that infiltrate tumors and detailed the manner in which anti-CD40/anti–CSF-1R immunotherapy altered endogenous immunity. Tumors treated with both anti-CD40 and anti–CSF-1R maintained features of both monotherapies, but the combination regimen increased the magnitude of changes in myeloid and lymphoid responses. Our data highlight how successful antitumor efficacy might require both the removal of suppressive populations and the delivery of activating signals for immune cells in the TME. The cumulative effect of CD40 agonism and CSF-1R inhibition conditions immune infiltrates to counteract immunosuppression in the tumor environment and successfully attack tumor cells.

Disclosure of Potential Conflicts of Interest

M. Quigley has ownership interest in Bristol-Myers Squibb. No potential conflicts of interest were disclosed by the other authors.

Authors' Contributions

Conception and design: K.R. Wiehagen, N.M. Girgis, D.H. Yamada, I.S. Grewal, M. Quigley, R.I. Verona
Development of methodology: K.R. Wiehagen, N.M. Girgis, D.H. Yamada
Acquisition of data (provided animals, acquired and managed patients, provided facilities, etc.): K.R. Wiehagen, N.M. Girgis
Analysis and interpretation of data (e.g., statistical analysis, biostatistics, computational analysis): K.R. Wiehagen, N.M. Girgis, D.H. Yamada, A.A. Smith, S.R. Chan, I.S. Grewal, M. Quigley, R.I. Verona
Writing, review, and/or revision of the manuscript: K.R. Wiehagen, D.H. Yamada, A.A. Smith, S.R. Chan, I.S. Grewal, M. Quigley, R.I. Verona
Administrative, technical, or material support (i.e., reporting or organizing data, constructing databases): K.R. Wiehagen, A.A. Smith
Study supervision: K.R. Wiehagen, I.S. Grewal, M. Quigley, R.I. Verona

Acknowledgments

The authors acknowledge the contributions of Cassandra L. Lowenstein, Nikki A. DeAngelis, and Catherine A. Ferrante in support of *ex vivo* experiments. Amy Wong, Leopoldo L. Luistro, Darlene J. Pizutti, and Diana Chin supported *in vivo* studies. We thank Enrique Zudaire and Jonathan Cenna for expert advice and helpful discussions, and Enrique Zudaire for critical reading of this article.

The costs of publication of this article were defrayed in part by the payment of page charges. This article must therefore be hereby marked *advertisement* in accordance with 18 U.S.C. Section 1734 solely to indicate this fact.

Received May 22, 2017; revised September 1, 2017; accepted October 24, 2017; published OnlineFirst November 2, 2017.

References

1. Palucka AK, Coussens LM. The basis of oncoimmunology. Cell 2016; 164:1233–47.
2. Galdiero MR, Bonavita E, Barajon I, Garlanda C, Mantovani A, Jaillon S. Tumor associated macrophages and neutrophils in cancer. Immunobiology 2013;218:1402–10.
3. Hoves S, Krause SW, Schutz C, Halbritter D, Scholmerich J, Herfarth H, et al. Monocyte-derived human macrophages mediate anergy in allogeneic T cells and induce regulatory T cells. J Immunol 2006;177:2691–8.
4. Stanley ER, Chitu V. CSF-1 receptor signaling in myeloid cells. Cold Spring Harb Perspect Biol 2014;6. pii: a021857. doi: 10.1101/cshperspect.a021857.

5. Mantovani A, Sozzani S, Locati M, Allavena P, Sica A. Macrophage polarization: tumor-associated macrophages as a paradigm for polarized M2 mononuclear phagocytes. Trends Immunol 2002;23:549–55.
6. Priceman SJ, Sung JL, Shaposhnik Z, Burton JB, Torres-Collado AX, Moughon DL, et al. Targeting distinct tumor-infiltrating myeloid cells by inhibiting CSF-1 receptor: combating tumor evasion of antiangiogenic therapy. Blood 2010;115:1461–71.
7. Wynn TA, Chawla A, Pollard JW. Macrophage biology in development, homeostasis and disease. Nature 2013;496:445–55.
8. Gordon S, Martinez FO. Alternative activation of macrophages: mechanism and functions. Immunity 2010;32:593–604.
9. Kurahara H, Shinchi H, Mataki Y, Maemura K, Noma H, Kubo F, et al. Significance of M2-polarized tumor-associated macrophage in pancreatic cancer. J Surg Res 2011;167:e211–9.
10. Beck AH, Espinosa I, Edris B, Li R, Montgomery K, Zhu S, et al. The macrophage colony-stimulating factor 1 response signature in breast carcinoma. Clin Cancer Res 2009;15:778–87.
11. Espinosa I, Beck AH, Lee CH, Zhu S, Montgomery KD, Marinelli RJ, et al. Coordinate expression of colony-stimulating factor-1 and colony-stimulating factor-1-related proteins is associated with poor prognosis in gynecological and nongynecological leiomyosarcoma. Am J Pathol 2009;174:2347–56.
12. Mitchem JB, Brennan DJ, Knolhoff BL, Belt BA, Zhu Y, Sanford DE, et al. Targeting tumor-infiltrating macrophages decreases tumor-initiating cells, relieves immunosuppression, and improves chemotherapeutic responses. Cancer Res 2013;73:1128–41.
13. Zhu Y, Knolhoff BL, Meyer MA, Nywening TM, West BL, Luo J, et al. CSF1/CSF1R blockade reprograms tumor-infiltrating macrophages and improves response to T-cell checkpoint immunotherapy in pancreatic cancer models. Cancer Res 2014;74:5057–69.
14. Sluijter M, van der Sluis TC, van der Velden PA, Versluis M, West BL, van der Burg SH, et al. Inhibition of CSF-1R supports T-cell mediated melanoma therapy. PLoS One 2014;9:e104230.
15. Pyonteck SM, Akkari L, Schuhmacher AJ, Bowman RL, Sevenich L, Quail DF, et al. CSF-1R inhibition alters macrophage polarization and blocks glioma progression. Nat Med 2013;19:1264–72.
16. Strachan DC, Ruffell B, Oei Y, Bissell MJ, Coussens LM, Pryer N, et al. CSF1R inhibition delays cervical and mammary tumor growth in murine models by attenuating the turnover of tumor-associated macrophages and enhancing infiltration by CD8+ T cells. Oncoimmunology 2013;2:e26968.
17. Ries CH, Hoves S, Cannarile MA, Ruttinger D. CSF-1/CSF-1R targeting agents in clinical development for cancer therapy. Curr Opin Pharmacol 2015;23:45–51.
18. Beatty GL, Li Y, Long KB. Cancer immunotherapy: activating innate and adaptive immunity through CD40 agonists. Expert Rev Anticancer Ther 2017;17:175–86.
19. Posner MR, Cavacini LA, Upton MP, Tillman KC, Gornstein ER, Norris CM Jr. Surface membrane-expressed CD40 is present on tumor cells from squamous cell cancer of the head and neck in vitro and in vivo and regulates cell growth in tumor cell lines. Clin Cancer Res 1999;5:2261–70.
20. Schoenberger SP, Toes RE, van der Voort EI, Offringa R, Melief CJ. T-cell help for cytotoxic T lymphocytes is mediated by CD40-CD40L interactions. Nature 1998;393:480–3.
21. Toes RE, Schoenberger SP, van der Voort EI, Offringa R, Melief CJ. CD40-CD40Ligand interactions and their role in cytotoxic T lymphocyte priming and anti-tumor immunity. Semin Immunol 1998;10:443–8.
22. Grammer AC, Bergman MC, Miura Y, Fujita K, Davis LS, Lipsky PE. The CD40 ligand expressed by human B cells costimulates B cell responses. J Immunol 1995;154:4996–5010.
23. Carbone E, Ruggiero G, Terrazzano G, Palomba C, Manzo C, Fontana S, et al. A new mechanism of NK cell cytotoxicity activation: the CD40-CD40 ligand interaction. J Exp Med 1997;185:2053–60.
24. Henn V, Slupsky JR, Grafe M, Anagnostopoulos I, Forster R, Muller-Berghaus G, et al. CD40 ligand on activated platelets triggers an inflammatory reaction of endothelial cells. Nature 1998;391:591–4.
25. Bennett SR, Carbone FR, Karamalis F, Flavell RA, Miller JF, Heath WR. Help for cytotoxic-T-cell responses is mediated by CD40 signalling. Nature 1998;393:478–80.
26. Nowak AK, Robinson BW, Lake RA. Synergy between chemotherapy and immunotherapy in the treatment of established murine solid tumors. Cancer Res 2003;63:4490–6.
27. Ahonen CL, Doxsee CL, McGurran SM, Riter TR, Wade WF, Barth RJ, et al. Combined TLR and CD40 triggering induces potent CD8+ T cell expansion with variable dependence on type I IFN. J Exp Med 2004;199:775–84.
28. Murphy WJ, Welniak L, Back T, Hixon J, Subleski J, Seki N, et al. Synergistic anti-tumor responses after administration of agonistic antibodies to CD40 and IL-2: coordination of dendritic and CD8+ cell responses. J Immunol 2003;170:2727–33.
29. Liu C, Lewis CM, Lou Y, Xu C, Peng W, Yang Y, et al. Agonistic antibody to CD40 boosts the antitumor activity of adoptively transferred T cells in vivo. J Immunother 2012;35:276–82.
30. Byrne KT, Leisenring NH, Bajor DL, Vonderheide RH. CSF-1R-dependent lethal hepatotoxicity when agonistic CD40 antibody is given before but not after chemotherapy. J Immunol 2016;197:179–87.
31. Movahedi K, Laoui D, Gysemans C, Baeten M, Stange G, Van den Bossche J, et al. Different tumor microenvironments contain functionally distinct subsets of macrophages derived from Ly6C(high) monocytes. Cancer Res 2010;70:5728–39.
32. Georgoudaki AM, Prokopec KE, Boura VF, Hellqvist E, Sohn S, Ostling J, et al. Reprogramming tumor-associated macrophages by antibody targeting inhibits cancer progression and metastasis. Cell Rep 2016;15:2000–11.
33. Rakhmilevich AL, Alderson KL, Sondel PM. T-cell-independent antitumor effects of CD40 ligation. Int Rev Immunol 2012;31:267–78.
34. Saraiva M, O'Garra A. The regulation of IL-10 production by immune cells. Nat Rev Immunol 2010;10:170–81.
35. Sato T, Terai M, Tamura Y, Alexeev V, Mastrangelo MJ, Selvan SR. Interleukin 10 in the tumor microenvironment: a target for anticancer immunotherapy. Immunol Res 2011;51:170–82.
36. Quezada SA, Jarvinen LZ, Lind EF, Noelle RJ. CD40/CD154 interactions at the interface of tolerance and immunity. Annu Rev Immunol 2004;22:307–28.
37. Grewal IS, Flavell RA. The role of CD40 ligand in costimulation and T-cell activation. Immunol Rev 1996;153:85–106.
38. Roberts EW, Broz ML, Binnewies M, Headley MB, Nelson AE, Wolf DM, et al. Critical role for CD103(+)/CD141(+) dendritic cells bearing CCR7 for tumor antigen trafficking and priming of T cell immunity in melanoma. Cancer Cell 2016;30:324–36.
39. Hansen M, Andersen MH. The role of dendritic cells in cancer. Semin Immunopathol 2017;39:307–16.
40. Byrne KT, Vonderheide RH. CD40 stimulation obviates innate sensors and drives T cell immunity in cancer. Cell Rep 2016;15:2719–32.
41. Ries CH, Cannarile MA, Hoves S, Benz J, Wartha K, Runza V, et al. Targeting tumor-associated macrophages with anti-CSF-1R antibody reveals a strategy for cancer therapy. Cancer Cell 2014;25:846–59.
42. Li H, Shi B. Tolerogenic dendritic cells and their applications in transplantation. Cell Mol Immunol 2015;12:24–30.
43. Whitmire JK, Flavell RA, Grewal IS, Larsen CP, Pearson TC, Ahmed R. CD40-CD40 ligand costimulation is required for generating antiviral CD4 T cell responses but is dispensable for CD8 T cell responses. J Immunol 1999;163:3194–201.
44. Yang XO, Nurieva R, Martinez GJ, Kang HS, Chung Y, Pappu BP, et al. Molecular antagonism and plasticity of regulatory and inflammatory T cell programs. Immunity 2008;29:44–56.
45. Pauken KE, Wherry EJ. Overcoming T cell exhaustion in infection and cancer. Trends Immunol 2015;36:265–76.
46. Zarour HM. Reversing T-cell dysfunction and exhaustion in cancer. Clin Cancer Res 2016;22:1856–64.
47. Church SE, Jensen SM, Antony PA, Restifo NP, Fox BA. Tumor-specific CD4+ T cells maintain effector and memory tumor-specific CD8+ T cells. Eur J Immunol 2014;44:69–79.
48. Eissler N, Mao Y, Brodin D, Reutersward P, Andersson Svahn H, Johnsen JI, et al. Regulation of myeloid cells by activated T cells determines the efficacy of PD-1 blockade. Oncoimmunology 2016;5:e1232222.
49. Luheshi NM, Coates-Ulrichsen J, Harper J, Mullins S, Sulikowski MG, Martin P, et al. Transformation of the tumour microenvironment by a CD40 agonist antibody correlates with improved responses to PD-L1 blockade in a mouse orthotopic pancreatic tumour model. Oncotarget 2016;7:18508–20.
50. Zippelius A, Schreiner J, Herzig P, Muller P. Induced PD-L1 expression mediates acquired resistance to agonistic anti-CD40 treatment. Cancer Immunol Res 2015;3:236–44.